Self-Sustained Micromechanical Oscillator with Linear Feedback

Changyao Chen, Damián H. Zanette, Jeffrey R. Guest, David A. Czaplewski, and Daniel López

A self-sustained micro mechanical oscillator with linear feedback

Changyao Chen[1], Damián H. Zanette[2], Jeffrey R. Guest[1], David A. Czaplewski[1], Daniel López[1]

[1] *Center for Nanoscale Materials, Argonne National Laboratory, Lemont, USA, 60439*

[2] *Centro Atómico Bariloche and Instituto Balseiro,*
Comisión Nacional de Energía Atómica. Consejo Nacional de Investigaciones
Científicas y Técnicas. 8400 San Carlos de Bariloche, Argentina

Autonomous oscillators, such as clocks and lasers, produce periodic signals *without* any external frequency reference. In order to sustain stable periodic motions, there needs to be external energy supply as well as nonlinearity built into the oscillator to regulate the amplitude. Usually, nonlinearity is provided by the sustaining feedback mechanism, which also supplies energy, whereas the constituent resonator that determines the output frequency stays linear. Here we propose a new self-sustaining scheme that relies on the nonlinearity originating from the resonator itself to limit the oscillation amplitude, while the feedback remains linear. We introduce a model to describe the working principle of the self-sustained oscillations and validate it with experiments performed on a nonlinear microelectromechanical (MEMS) based oscillator.

Autonomous oscillators are systems that can spontaneously commence and maintain stable periodic signals in a self-sustained manner without external frequency references. They are abundant both in Nature and in manmade devices. In Nature made systems, the self-sustained oscillators are the fundamental piece that describes systems as diverse as neurons, cardiac tissue, and predator-prey relationships [1]. In manmade devices, self-sustained autonomous oscillators are overwhelmingly used for communications, timing, computation, and sensing [2], with examples such as quartz watches [3] and laser sources [4]. A typical oscillator consists of a resonating component and a sustaining feedback element: the constituent resonator determines the oscillation frequency, whereas the feedback system draws power from an external source to compensate the energy loss due to damping during each oscillation of the resonator [5]. In order to initiate the oscillations, the initial gain of the feedback must be larger than unity, so that energy accumulates to build up oscillation amplitude [6]. However, to avoid ever increasing oscillations, some limiting mechanism must act to ensure that, eventually, the vibrational amplitude no longer grows.

In the conventional designs of oscillators, the resonating element is operated in the linear regime, where its resonant frequency is independent of the excitation levels, and the necessary amplitude limiting mechanism is enacted in the feedback loop by introducing a nonlinear element (Fig. 1a). However, maintaining the resonating element in the linear regime has been challenging for a variety of applications requiring self-sustained oscillators made from micro-/nano-electromechanical (M/NEMS) resonators [7–9], mostly because these resonators exhibit significantly reduced linear dynamic range. To limit the amplitude, common mechanisms include impulsive energy replenishment [5], saturated gain medium [4, 10] or amplifiers [11, 12], automatic level control [13, 14], phase locked loops [15, 16], nonlinear signal transduction [17], and dedicated nonlinear components [18]. These mechanisms to incorporate nonlinear elements into the electronic feedback circuitry introduce technical challenges in the analysis, design and implementation of the oscillators due to the significant impedance mismatch between CMOS drivers and M/NEMS resonators [19].

In this Letter, we introduce and analyze a new oscillator architecture that solely relies on the nonlinearity originated from a micromechanical resonator, while all components of the feedback circuitry stay within the *linear* regime (Fig. 1b). By capitalizing on the intrinsic nonlinear dynamics of the mechanical resonator, it is possible to considerably simplify the design of the oscillator while achieving a large degree of control and tunability. Unlike the techniques used with linear resonators, the oscillator architecture we are proposing can be readily implemented in practically all M/NEMS geometries, as the only requirement is the existence of a nonlinear response. The proposed innovative architecture permits to (1) initiate the oscillation spontaneously, (2) achieve stable oscillations through interplay between elastic nonlinearities and viscous damping, and (3) tune the oscillation frequency over a wide range with readily accessible system parameters. We demonstrate this new architecture with an oscillator consisting of a clamped-clamped (c-c) silicon MEMS resonator [16] with high quality factor ($Q \gtrsim 10^5$), and with frequency tunability as large as 19 %.

We treat the mechanical resonator as a generic single degree-of-freedom oscillating element, whose departure from equilibrium is described by a coordinate $x(t)$ obeying [20]:

$$m\ddot{x} + (\gamma + \tilde{\eta}x^2)\dot{x} + m\omega_0^2 x + \tilde{\beta}x^3 = F(x, \dot{x}), \quad (1)$$

where m is the effective mass, γ and $\tilde{\eta}$ are the linear and nonlinear damping coefficients [21, 22], ω_0 is the natural frequency of linear oscillation, $\tilde{\beta}$ is the cubic (Duffing) nonlinear coefficient, and $F(x, \dot{x})$ is the driving force from feedback. Since we only focus on periodic solutions, quadratic nonlinearities are ignored. To facil-

itate the analysis, we define $\epsilon q^{-1} = \gamma/m\omega_0$, $\eta = \tilde{\eta}/4\gamma$, $\beta = 3\tilde{\beta}/4m\omega_0^2$, and a fast time scale $\tau = \omega_0 t$. Here, the small expansion parameter ϵ is introduced for treatment within a perturbation theory, as shown below. Since the feedback force, F, is only needed to compensate the dissipation, it will also be of the order of ϵ. Furthermore, we treat the feedback force as proportional to the vibrational amplitude, corresponding to the cases where the vibrational amplitude is linearly transduced and directly measured experimentally. Similarly, the feedback force can be treated as proportional to the vibrational velocity, if the velocity is the observed quantity as in the case of capacitive motion transduction [23]. For simplicity, here we consider the case of linear amplitude amplification and scale the feedback force as $F = \epsilon m\omega_0^2 g x \cos\Delta$, where g is the feedback gain and Δ the feedback loop phase-delay. With these definitions, Eq. (1) becomes

$$\ddot{x} + \epsilon q^{-1}(1 + 4\eta x^2)\dot{x} + x + \frac{4}{3}\beta x^3 = \epsilon g x \cos\Delta. \quad (2)$$

Here the time derivatives are calculated with respect to τ.

We represent the limit of small dissipation by taking $\epsilon \ll 1$, and the scaled quality factor q of the order of unity. The solution to Eq. (2) can be found through perturbation theory [24]. However, in contrast with previous treatments with weak nonlinearity [20], we do not assume that the cubic force is small as compared to the linear term [25]. The resulting zeroth-order equation is therefore the nonlinear Duffing equation without damping: $\ddot{x}_0 + x_0 + \frac{4}{3}\beta x_0^3 = 0$. We propose a steady-state solution of the form $x_0 = A_0 \cos\Omega_0\tau$, where A_0 and Ω_0 are the oscillation amplitude and frequency of the zeroth-order solution, respectively. By neglecting higher-harmonics contributions, we find that A_0 and Ω_0 must satisfy the relation

$$1 - \Omega_0^2 + \beta A_0^2 = 0. \quad (3)$$

Following the method of multiple time-scales [23, 24], we proceed to obtain the steady-state solution to Eq. (2) up to $O(\epsilon)$. This solution will be characterized by amplitude A and frequency ω, determined both by intrinsic properties (β, η, q) and extrinsic parameters Δ, g [23]. Fig. 1c and 1d illustrate the relation between the steady-state amplitude A and frequency ω, for different values of feedback excitations and Δ. For small excitations (Fig. 1c), we recover the resonance curve as obtained for weakly nonlinear resonators [20]. For large excitation (Fig. 1d), where the oscillation frequency is pulled far away from the linear resonance ($\omega - 1 \gg \epsilon$), the perturbed solution is practically identical to that of zeroth-order equation Eq. (3). It is worth noting that, in the case of our autonomous oscillator, both the amplitude A and the frequency ω are functions of the phase delay Δ. Therefore, if multiple solutions of A exist for a given
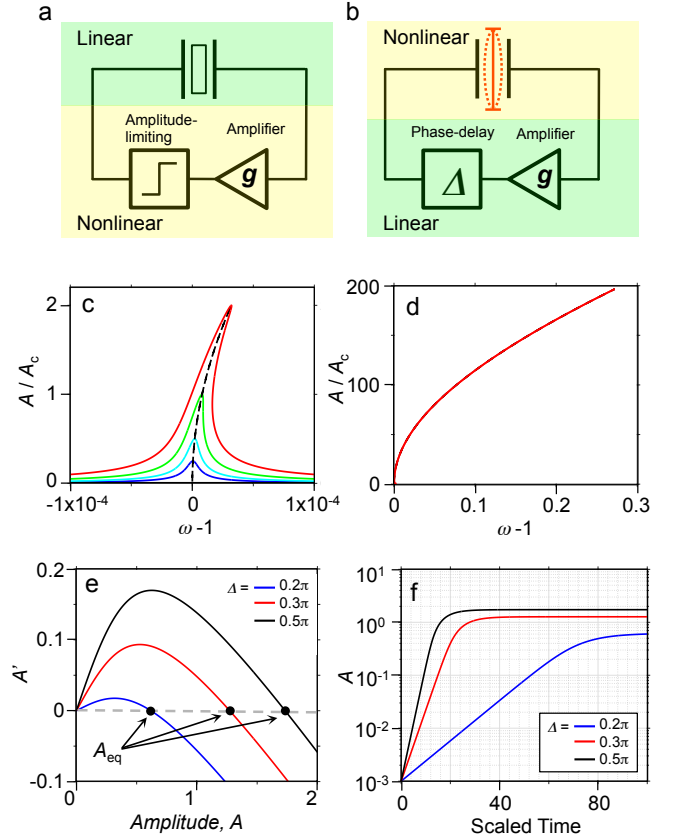

FIG. 1. (a) Schematics of the conventional oscillator design, consisting of a linear resonator and nonlinear feedback. The output of the resonator is first amplified, and then amplitude-limited before being fed-back to the resonator. (b) Schematics of oscillator design with a nonlinear resonator and linear feedback loop. The output of the resonator is amplified and phase shifted, and then re-injected to the resonator. (c) Vibrational amplitude A (expressed as the ratio to the critical amplitude A_c, above which multiple solutions exist) versus frequency detuning in the limit of small drive, derived from Eq. (2), with $\epsilon = 10^{-5}$, $\beta = 1$, $\eta = 0$, and different levels of excitation. The dashed backbone curve shows the solution to Eq. (3). (d) Same results but with large excitation, where the full solution practically coincides with the backbone. (e) Phase portrait of amplitude A, showing unstable rest states, and different stable equilibrium A_{eq} at various Δ. (f) Simulated transient responses of A at different Δ.

value of ω, all of them are stable [23, 26], as opposed to an externally driven resonator where only two solutions are stable. Moreover, nonlinearities make it possible to achieve frequencies far above the linear oscillation frequency, only bounded by other nonlinearities present in the system, or by physical limits of the device.

For hardening nonlinearity ($\beta > 0$), closer inspection of the full solution reveals that the zero-amplitude state for our system is unstable, as indicated by the phase portrait shown in Fig. 1e: any disturbance will push the oscillator away from rest state, towards the stable equilibrium A_{eq},

marked by the arrows in Fig. 1e. Physically, this stable equilibrium can be understood as the energy balance between driving and damping: if the amplitude A increases suddenly around A_{eq}, (for instance, by noise), due to the proportionality between the forcing and the amplitude there is a growth in the input energy. At the same time, because of the hardening nonlinearity, the increased amplitude pushes the oscillation frequency ω upward, resulting in a larger energy dissipation due to viscous damping, which is proportional to the product of $A\omega$. The energy balance is thus restored, and the oscillation amplitude achieves a steady state (Fig. 1f). A symmetric argument holds if the amplitude decreases. We have also examined the case where the feedback force is proportional to velocity, and arrived at similar conclusion [23]. In this case, however, the balance is maintained by the effects of nonlinear damping, which becomes stronger as the oscillation amplitude grows. This energy balance highlights the key difference with previous oscillator topologies with a dedicated amplitude limiting element [12, 16, 18]. In the current setup, intrinsic nonlinearities are an indispensable ingredient for stabilization. Additionally, the spontaneous oscillation greatly simplifies the startup protocol of the oscillator, making it highly suitable for M/NEMS based oscillators where very sensitive transducers are required to initiate the motion.

We used a MEMS based oscillator to experimentally demonstrate these concepts. The resonator, similar to the one used in [16], is placed in a vacuum chamber and actuated electrostatically. The mechanical vibration creates a capacitive current in the sensing comb, that is proportional to the velocity. Both of the comb electrodes consist of 25 interdigitated fingers that allow efficient excitation and linear signal transduction. The measured linear resonance is 61.57 kHz, with linear damping rate of 0.51 Hz [23]. The small dissipation of $\epsilon^{-1} = Q \sim 120,000$ ensures that the resonator is well suited for the designed nonlinear oscillator. In this case, the nonlinearity is geometrical in origin and arises from the elongation of the beam during large transverse vibration. The onset of nonlinearity x_c - above which the amplitude-frequency relation bifurcates - is calculated to be 17 nm from the geometry of the device [8], and experimentally found to be about 10 nm [23]. In the experiments, we have observed oscillation amplitudes larger than 1 μm, well above the linear threshold. We find excitations larger than 100 μV are enough to drive the resonator into the nonlinear regime. When the resonator is excited with an even larger force, it displays the signature of nonlinear damping [20, 23, 27, 28].

The feedback loop consists of a transimpedance amplifier followed by a voltage amplifier and a band pass filter. Therefore, the feedback force is proportional to the velocity with a certain phase-delay. In order to ensure the linearity of the feedback loop, we have calibrated the linearity of each component in the feedback circuitry,
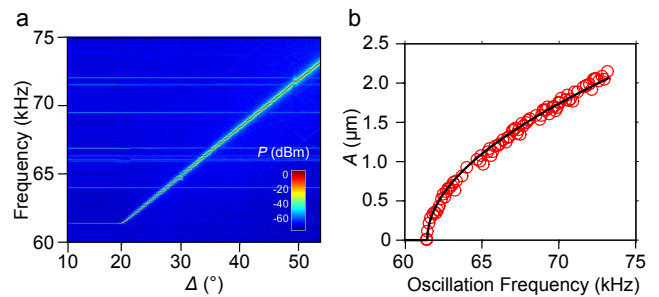

FIG. 2. Steady-state response of a nonlinear oscillator. (a) Measured power spectrum of the oscillation with different feedback-phase-delay Δ. Measurement at each Δ is performed with a time constant long enough to ensure the transient response has died out. The DC bias is 7 V. (b) Extracted steady-state oscillation amplitude and frequency (red circles), and fitting to Eq. (3), with $\beta = 1.15 \times 10^{11} \text{m}^{-2}$.

and found all of them operating in the linear regime [23]. Operating the electronics in the linear regime provides a large range of operational voltages that allows for significant detuning of the MEMS. Additionally, eliminating complex controlling circuits for oscillators [29] greatly reduces the number of elements in the feedback loop, lowering the power consumption [30].

Figure 2a shows the steady-state power spectrum of the oscillation, measured at different phase-delay Δ. For $\Delta < 20°$, no oscillation is observed, whereas for $\Delta > 20°$, the oscillations occur and the frequency grows monotonically with Δ. This is consistent with the fact that, in order to initiate spontaneous oscillations, the feedback force should overcome damping. The onset of the oscillation frequency is about 61.5 kHz, slightly above the linear resonance, and the highest oscillation frequency observed is 73.15 kHz, which is about 19 % above the linear resonance. We are hindered by the instrumental limit from achieving larger phase-delay and frequency detuning. The acquisition time of each spectrum is much longer than the transient time of the oscillation, to ensure steady-state conditions. The oscillation amplitude versus frequency (Fig. 2b) clearly shows the quasi-square-root dependency, as predicted by Eq. (3). The scaled Duffing nonlinearity β, obtained from fitting to Eq. (3), is $1.15 \times 10^{11} \text{m}^{-2}$, in good agreement with previous result [31].

Next we consider the buildup of the oscillation. The spontaneous initiation of the oscillating motion with linear feedback does not require the prerequisite of the Barkhausen criterion [18]: after the amplified and phase-shifted signal is fed back to actuate the resonator, the system will asymptotically transition to the stable limit cycle, whose frequency can be controlled by g and Δ [23]. Fig. 3 shows the temporal evolution of the oscillator during the startup: after the feedback is engaged at $t = 0$ s, the envelope of oscillation amplitude, A,
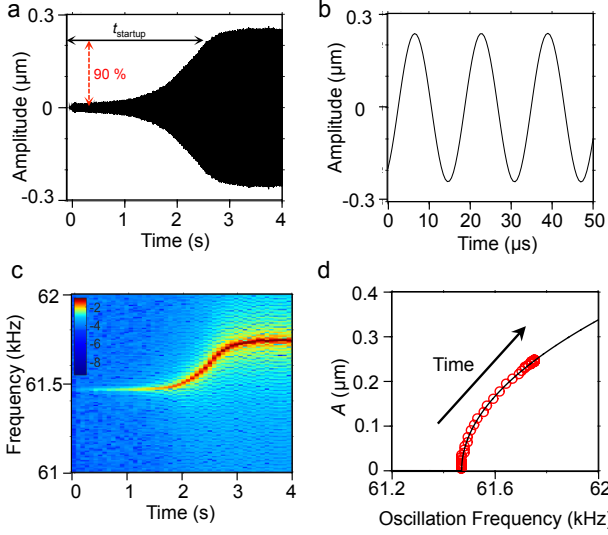
FIG. 3. Transient response during startup. (a) Measured amplitude during oscillation buildup. The steady-state oscillation frequency is 61.7 kHz, with $\Delta = 24.1°$. (b) Zoomed-in view of the steady-state oscillation of (a). The x-axis is shifted arbitrarily. (c) Temporal frequency response of the oscillation. The power spectrum at each nominal time t_i is obtained by performing non-overlapping fast Fourier transform (FFT) of the time domain data in a narrow window around t_i. (d) The temporal evolution of the oscillator on the amplitude-frequency plane, and fitting to Eq. (3) (black solid line). The extracted β is $1.05 \times 10^{11} \mathrm{m}^{-2}$. The DC bias is 7 V for all the data shown.

grows rapidly towards the final value (Fig. 3a). The steady-state response shows stable sinusoidal oscillation, as shown in Fig. 3b. The temporal frequency evolution shows a similar pattern (Fig. 3c, corresponding to the time domain data shown in Fig. 3a): the instantaneous frequency starts at the linear resonant frequency value, and shifts upward towards the steady-state oscillation frequency. This temporal evolution is shown on the amplitude-frequency plane (Fig. 3d), where we plot the amplitude-frequency of the oscillator every 80 miliseconds. It can be clearly seen that the temporal response of the oscillator follows the prescribed square-root interdependence, Eq. (3), with an extracted $\beta = 1.05 \times 10^{11} \mathrm{m}^{-2}$. The inter-dependence between the vibrational amplitude and frequency underlines the working principle of the stable oscillation: any unintentional increase in amplitude will increase the resonant frequency of the resonator, which leads to more viscous damping, which in turn reduces the amplitude, hence maintaining the oscillations stable.

Finally, we will examine the influence of the system parameters on the oscillation buildup. We define the startup time, t_{startup}, as the time needed for the oscillation amplitude to reach 90% of its steady-state value. We find that t_{startup} drops considerably with increasing
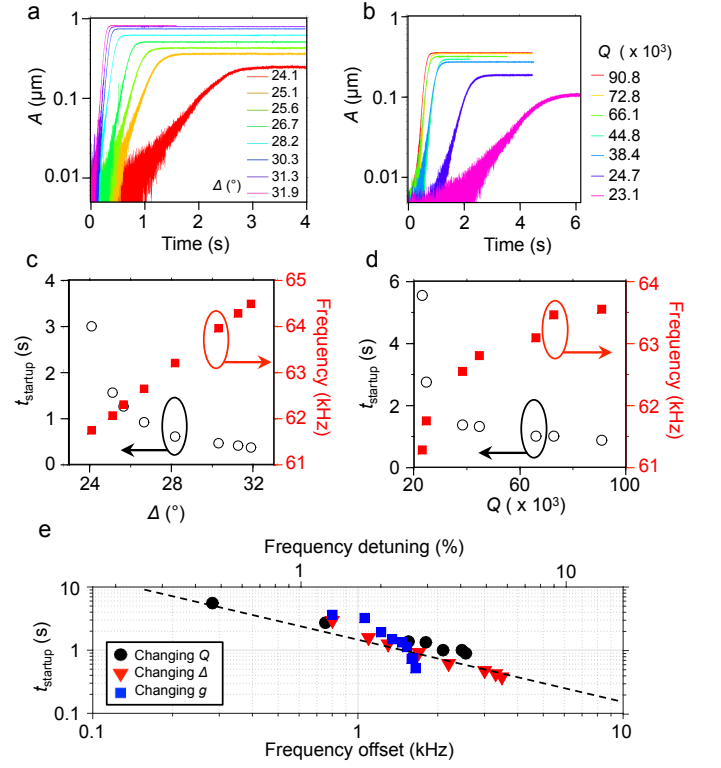

FIG. 4. Control of oscillation startup. (a) Envelope of the amplitude during startup, for different Δ, with $Q = 120,000$. The envelope is obtained through averaging of multiple cycles of the oscillation around given times. (b) Envelope of the amplitude during startup, for different Q, with $\Delta = 27°$. (c, d) Corresponding startup time t_{startup} and steady-state frequency extracted from (a) and (b), respectively. (e) The startup time t_{startup} versus steady state frequency offset, collected with different startup conditions. The dashed line is a guide to the eyes with slope of -1.

the phase-delay Δ (Fig. 4a, c), which is consistent with the theoretical modeling considering the feedback force is proportional to g and Δ [23]. Additionally, we also modify the effective gain g by changing the DC bias and observe a similar dependence of t_{startup} [23].

To validate the model against intrinsic properties of the resonator, we deliberately tune the linear damping rate γ by increasing the pressure of the vacuum chamber, which changes the quality factor Q. The values of Q are obtained from separated open-loop resonator-type measurements [23]. The startup time increases drastically when Q drops below $\sim 30,000$ (Fig. 4b, d), and we failed to observe any oscillation for $Q < 10,000$.

Since the only requirement for this oscillator topology to work is to have the resonator in the nonlinear regime, self-sustained oscillations can be achieved at low values of Q by changing the dimensions of the resonator. The onset of nonlinearity scales with the characteristic length of the resonating element, and for NEMS devices, even forces from thermal noise can drive the resonator into the

nonlinear regime [32].

The startup time, obtained from different system configurations, is shown in Fig. 4e, and is found to be approximately inversely proportional to the steady state frequency offset. This observation highlights another benefit of the new topology: the more nonlinear the response is, the shorter the startup time. The nonlinear mechanical resonator ensures stable oscillation, whose frequency offset is proportional to the total feedback gain, whereas the linear feedback allows for exponentially fast transient towards the stable oscillation, which results in shorter startup time with larger gain.

In summary, we have introduced a novel oscillator architecture consisting of a nonlinear mechanical resonator driven by a linear feedback loop. We have theoretically examined the conditions for stable periodic motion and have shown that when the feedback forcing is proportional to the vibration amplitude, a hardening nonlinear response ensures the balance between external energy input and intrinsic dissipation necessary to stabilize oscillations. The interplay between the resonator's frequency dependent amplitude and the associated damping underlines the principle of stable oscillations. When the feedback forcing is proportional to the oscillation velocity, in turn, the balance is guaranteed by nonlinear damping.

As the size of the resonating elements shrinks towards the nanoscale, the critical amplitudes for onset of nonlinearity decreases accordingly [8, 33] and the resonators will inevitably operate in the mechanical nonlinear regime, even merely driven by thermal noise[32]. Since the mechanical nonlinearities of the resonator are responsible for achieving self-sustained oscillations, the new architecture should perform better when scaled down to the nanoscale [34], making it ideal for oscillators incorporating nanoscale resonators and for very large-scale integration of high-Q MEMS and NEMS.

[1] S. H. Strogatz, *Nonlinear dynamics and chaos: with applications to physics, biology, chemistry, and engineering* (Westview press, 2014).

[2] A. Jenkins, Physics Reports **525**, 167 (2013).

[3] C. Audoin and B. Guinot, *The measurement of time: time, frequency and the atomic clock* (Cambridge University Press, 2001).

[4] T. H. Maiman, Nature **187**, 493 (1960).

[5] A. Andronov, A. Vitt, and S. Khaikin, *Theory of oscillators*, Dover Books on Electrical Engineering (Dover Publications, 1966).

[6] H. Barkhausen, *Lehrbuch der Elektronenröhren und ihrer technischen Anwendungen* (Hirzel, 1963).

[7] A. K. Naik, M. S. Hanay, W. K. Hiebert, X. L. Feng, and M. L. Roukes, Nature Nanotechnology **4**, 445 (2009).

[8] K. L. Ekinci and M. L. Roukes, Review of Scientific Instruments **76**, 061101 (2005).

[9] F. Cottone, H. Vocca, and L. Gammaitoni, Physical Review Letters **102**, 080601 (2009).

[10] A. L. Schawlow and C. H. Townes, Physical Review **112**, 1940 (1958).

[11] E. Vittoz, *Low-power crystal and MEMS oscillators: the experience of watch developments* (Springer Science & Business Media, 2010).

[12] X. Feng, C. White, A. Hajimiri, and M. L. Roukes, Nature nanotechnology **3**, 342 (2008), after private communication with the author, one of the sustaining amplifier is saturated.

[13] S. Lee and C. T.-C. Nguyen, in *Frequency Control Symposium and PDA Exhibition Jointly with the 17th European Frequency and Time Forum, 2003. Proceedings of the 2003 IEEE International* (IEEE, 2003) pp. 341–349.

[14] Y.-W. Lin, S. Lee, S.-S. Li, Y. Xie, Z. Ren, and C.-C. Nguyen, Solid-State Circuits, IEEE Journal of **39**, 2477 (2004).

[15] F. J. Giessibl, Reviews of modern physics **75**, 949 (2003).

[16] D. Antonio, D. H. Zanette, and D. López, Nature communications **3**, 806 (2012).

[17] C. T.-C. Nguyen and R. T. Howe, Solid-State Circuits, IEEE Journal of **34**, 440 (1999).

[18] L. G. Villanueva, R. B. Karabalin, M. H. Matheny, E. Kenig, M. C. Cross, and M. L. Roukes, Nano Lett. **11**, 5054 (2011).

[19] J. Van Beek and R. Puers, Journal of Micromechanics and Microengineering **22**, 013001 (2011).

[20] R. Lifshitz and M. C. Cross, in *Reviews of Nonlinear Dynamics and Complexity* (Wiley-VCH Verlag GmbH & Co. KGaA, 2009) pp. 1–52.

[21] M. Dykman and M. Krivoglaz, physica status solidi (b) **68**, 111 (1975).

[22] M. Dykman, *Fluctuating nonlinear oscillators: from nanomechanics to quantum superconducting circuits* (OUP Oxford, 2012).

[23] See Supplementary Information, which includes Refs. [35-36].

[24] A. H. Nayfeh and D. T. Mook, *Nonlinear oscillations* (John Wiley & Sons, 2008).

[25] S. I. Arroyo and D. H. Zanette, The European Physical Journal B **89**, 1 (2016).

[26] L. G. Villanueva, E. Kenig, R. B. Karabalin, M. H. Matheny, R. Lifshitz, M. C. Cross, and M. L. Roukes, Phys. Rev. Lett. **110**, 177208 (2013).

[27] M. Imboden and P. Mohanty, Physics Reports **534**, 89 (2014).

[28] P. M. Polunin, Y. Yang, M. I. Dykman, T. W. Kenny, and S. W. Shaw, Journal of Microelectromechanical Systems **PP**, 1 (2016).

[29] A. S. Sedra and K. C. Smith, *Microelectronic circuits*, Vol. 1 (New York: Oxford University Press, 1998).

[30] C.-C. Nguyen, Ultrasonics, Ferroelectrics and Frequency Control, IEEE Transactions on **54**, 251 (2007).

[31] D. Antonio, D. A. Czaplewski, J. R. Guest, D. López, S. I. Arroyo, and D. H. Zanette, Physical review letters **114**, 034103 (2015).

[32] J. Gieseler, L. Novotny, and R. Quidant, Nature Physics

9, 806 (2013).

[33] H. C. Postma, I. Kozinsky, A. Husain, and M. Roukes, Applied Physics Letters **86**, 223105 (2005).

[34] C. Chen, S. Lee, V. V. Deshpande, G.-H. Lee, M. Lekas, K. Shepard, and J. Hone, Nature Nano **8**, 923 (2013).

[35] I. Kovacic and M. J. Brennan, *The Duffing equation: nonlinear oscillators and their behaviour* (John Wiley & Sons, 2011).

[36] M. Imboden, O. A. Williams, and P. Mohanty, Nano letters **13**, 4014 (2013).